

Manganites at Quarter Filling: Role of Jahn-Teller Interactions

Jan Bała

*Max-Planck-Institut für Festkörperforschung, Heisenbergstrasse 1, D-70569 Stuttgart, Germany and
Marian Smoluchowski Institute of Physics, Jagellonian University, Reymonta 4, PL-30059 Kraków, Poland*

Peter Horsch and Frank Mack

Max-Planck-Institut für Festkörperforschung, Heisenbergstrasse 1, D-70569 Stuttgart, Germany

(Dated: October 30, 2018)

We have analyzed different correlation functions in a realistic spin-orbital model for half-doped manganites. Using a finite-temperature diagonalization technique the CE phase was found in the charge-ordered phase in the case of small antiferromagnetic interactions between t_{2g} electrons. It is shown that a key ingredient responsible for stabilization of the CE-type spin and orbital-ordered state is the cooperative Jahn-Teller (JT) interaction between next-nearest Mn^{+3} neighbors mediated by the breathing mode distortion of Mn^{+4} octahedra and displacements of Mn^{+4} ions. The topological phase factor in the Mn-Mn hopping leading to gap formation in one-dimensional models for the CE phase as well as the nearest neighbor JT coupling are not able to produce the zigzag chains typical for the CE phase in our model.

PACS numbers: 75.30.Kz, 71.70.Ej, 75.30.Et, 75.10.-b

I. INTRODUCTION

Half-doped perovskite manganites $Re_{1/2}A_{1/2}MnO_3$ (Re=rare earth, A=alkaline earth) exhibit very specific properties quite different from manganites with other e_g electron concentrations.^{1,2} Generally, for large size Re and A cations or when external pressure is applied³ these compounds are in the A-type antiferromagnetic (AF), metallic state at low temperatures showing no or only weak sign of charge ordering, and the occupied e_g electron states are predominantly x^2-y^2 like. Recently it has been reported that the A-phase may develop an intrinsic charge-stripe modulation, which controls the transport properties.⁴ With decreasing size of the cations, which implies a decrease of the bandwidth, charge ordering is observed which at lower temperatures is accompanied by the formation of peculiar ferromagnetic (FM) zigzag chains^{5,6,7} that are staggered antiferromagnetically. This CE spin order, a notation introduced in the pioneering work of Wollan and Koehler⁸ and Goodenough⁹, is accompanied by a checkerboard charge order (CO) and directed occupied orbitals on the Mn^{3+} sites amplifying double exchange (DE) along one lattice diagonal. The CE-structure is a particularly fascinating manifestation of the control of magnetic order due to the orbital degree of freedom^{10,11} in combination with charge ordering. Although a number of approaches have been followed to explain this structure, the mechanism for its stability is still not clear and hotly debated with emphasis put on the role of the DE,^{12,13,14} the Coulomb interaction,^{15,16,17,18} or the coupling to the lattice degrees of freedom.^{19,20,21,22,23,24,25}

The CE phase has been observed experimentally both in cubic $(Nd,Pr)_{1/2}(Sr,Ca)_{1/2}MnO_3$ ^{2,7,26,27,28} and in layered $LaSr_2Mn_2O_7$ ²⁹ and $La_{1/2}Sr_{3/2}MnO_4$ ^{5,6} manganites. In some cases it can coexist with the A-type AF spin ordering.^{29,30,31} Regarding CO in the CE phase, some

experiments are interpreted in terms of almost perfect CO^{6,32} while others³³ are considered to be consistent with a smooth charge density wave (CDW) of the e_g electron density. Although, it is plausible that the complex spin and orbital arrangement in the charge-ordered manganites can result from the competition between DE³⁴ and AF superexchange interactions ($\sim J_{AF}$), the role played by the CO and Jahn-Teller (JT) interactions^{20,21,22,35} in the system is still unclear. Finally in systems like e.g. $Pr_{1/2}Ca_{1/2}MnO_3$ CO and CE-type orbital correlations are found to develop well above the Neel temperature^{36,37} or even coexist with FM spin state,³⁸ which indicates that these orbital correlations are not primarily driven by magnetic interactions.

This work focuses on a microscopic understanding of the stability of the CE-phase which appears to be the ground state of narrow band manganites at and near quarter-filling. We argue here that the key interaction, apart from the nearest-neighbor Coulomb repulsion V which supports the charge ordering,³⁹ is the next-nearest neighbor JT interaction. This interaction between orbitals at next-nearest neighbor Mn^{3+} ions emerges from the JT-distortions of the Mn^{3+} octahedra which is amplified by the breathing distortion of the intermediate Mn^{+4} octahedra. We show that this interaction generates a narrow regime in the $V-J_{AF}$ phase diagram where the CE-phase (and sometimes the C-phase) is stable. Otherwise one encounters a homogeneous FM phase at small J_{AF} fully controlled by DE and a conventional nearest-neighbor AF phase at larger J_{AF} .

An important feature of further neighbor JT interactions are the displacements of the Mn^{+4} ions. We are only aware of work by Radaelli *et al.*⁴⁰ where detailed lattice coordinates for the CE-phase in $La_{1/2}Ca_{1/2}MnO_3$ are reported. In particular they observed that the 4 planar O(2) move towards the Mn^{+4} ion and the Mn^{+4} ions are found to be displaced from their regular perovskite posi-

tions, while the Mn^{3+} ions are not shifted. This observation confirms the importance of the breathing distortion and also shows the mechanism of the further neighbor JT-distortion in the CE-phase. As a consequence the appearance of new Bragg reflections in the CE-phase would be associated not primarily with quadrupolar electronic orbital order but rather with the displacements of ions associated with the CE orbital order.⁴⁰

An alternative long-ranged JT based interaction was recently proposed by Khomskii and Kugel⁴¹ and by Calderon, Millis and Ahn.⁴² They employ elasticity theory to derive the orbital interaction between JT-distorted Mn^{3+}O_6 octahedra for the perfectly charge ordered case. We have also investigated the consequences of this interaction. Our numerical simulations confirm the estimate presented in Ref. 41 that for perfect charge ordering the AF CE phase is stable. Yet in this model this requires large nearest neighbor Coulomb repulsion V , while for moderate values of V the CE phase gets unstable.

The finite temperature diagonalization^{16,43,44} used in our study allows to include the full interplay of spin and orbital states, and to monitor the onset of different orders as function of temperature. This gives us the ability for an unbiased investigation of the formation of different spin-orbital orderings emerging from all multi-electron configurations in the cluster. In this paper we concentrate on the stability and temperature dependence of spin, orbital, and charge ordered states in the two-dimensional (2D) realistic model for half-doped manganites. In our microscopic spin-orbital model CO develops as a result of nearest-neighbor Coulomb repulsion V and as a consequence of further neighbor JT interactions, while the spin-orbital order results from the competition between DE (i.e. kinetic energy), AF superexchange and further neighbor JT interactions. As shown in Sec. III D the latter interaction can lead to a CO state at low temperatures even in the absence of inter-site Coulomb repulsion. Furthermore we argue that a topological sign in the hopping amplitudes of e_g orbitals¹³ invoked in one-dimensional (1D) models for the CE phase is not sufficient to explain the formation of CE spin-orbital structure in the 2D model studied by us.

Further motivations to put effort in a better understanding of the interplay of spin, charge, orbitals and lattice in the formation of the CE-phase are the following: It has been argued that the intrinsic mechanism that leads to colossal magnetoresistance are tendencies towards CE-type charge and orbital ordering in the vicinity of $x = 0.5$.⁴⁵ Furthermore a CE-insulator to FM-metal transition has been observed in relatively small magnetic field, which is accompanied by a major change of the optical conductivity on a surprisingly large energy scale (~ 1 eV).^{46,47} Such dramatic changes in relatively weak magnetic fields are a clear manifestation of the subtle interplay between spin, orbital and CO. The present study provides a basis for further investigations of the temperature dependence of e.g. the optical conductivity and the study of spin and orbital excitations in the CE-phase, as

well as the effect of doping into the quarter filled state.

The paper is organized as follows. In Sec. II we present the model Hamiltonian, and describe in Sec. II B the finite-temperature Lanczos method. Sec. III contains numerical results for different two-site correlation functions characterizing the charge, orbital and spin structure. These correlation functions are evaluated as functions of temperature and collected in a form of semi-quantitative phase diagrams in three different regimes: (i) including nearest-neighbor effective orbital-orbital (OO) interactions (Sec. III B); (ii) assuming the elastic form of OO coupling at different distances (Sec. III C); (iii) considering the local form of next- and nearest-neighbor OO coupling (Sec. III D), while in Sec. III F the effect of charge stacking is discussed. The paper is summarized in Sec. IV. In the Appendix the stability of the CE versus the C phase is analysed for a 1D band model with lifted orbital degeneracy.

II. MODEL HAMILTONIAN AND NUMERICAL PROCEDURE

A. Effective spin-orbital model

We consider the generic FM Kondo lattice model for manganites^{43,44} with the Mn e_g electrons coupled to the core t_{2g} spins via the Hund coupling J_H . The model is augmented by inter-site Coulomb repulsion V and cooperative JT interactions and treated in the limit of infinite on-site Coulomb repulsion between two e_g electrons on the same site ($U \rightarrow \infty$):

$$H = H_{band} + H_{Kondo} + H_{AF} + H_V + H_{OO}. \quad (1)$$

The first term describes the motion of the e_g electrons,

$$H_{band} = - \sum_{\langle ij \rangle \xi \zeta, \sigma} \left(t_{ij}^{\xi \zeta} \tilde{d}_{i\xi\sigma}^\dagger \tilde{d}_{j\zeta\sigma} + \text{H.c.} \right), \quad (2)$$

with a constraint that allows only for Mn^{4+} and Mn^{3+} configurations, $\tilde{d}_{i\xi\sigma}^\dagger = d_{i\xi\sigma}^\dagger (1 - n_{i\xi\sigma}) \prod_{\sigma'} (1 - n_{i\xi\sigma'})$, where all other alternative e_g states are projected out. Here and in the following the index $\bar{\xi}$ ($\bar{\sigma}$) denotes the e_g orbital (spin) orthogonal to the ξ (σ) one, respectively. The hopping matrix elements depend on the basis chosen. For the basis $\{|x\rangle, |z\rangle\}$ with $|x\rangle \sim x^2 - y^2$ and $|z\rangle \sim 3z^2 - r^2$ they are given by,

$$\left[t_{ij}^{\xi \zeta} \right]_{|a(b)} = \frac{t}{4} \begin{pmatrix} 3 & \mp \sqrt{3} \\ \mp \sqrt{3} & 1 \end{pmatrix}, \quad (3)$$

where, $+(-)$ refer to the $a(b)$ direction, respectively. The second term of Hamiltonian (1) stands for the Hund interaction between e_g electrons spin and the $S = 3/2$ t_{2g} core spin \mathbf{S}_i ,

$$H_{Kondo} = -J_H \sum_{i\xi\sigma\sigma'} \mathbf{S}_i \cdot \tilde{d}_{i\xi\sigma}^\dagger \vec{\sigma}_{\sigma\sigma'} \tilde{d}_{i\xi\sigma'}, \quad (4)$$

resulting in the parallel alignment of spins between t_{2g} and e_g electrons at each site in the limit $J_H \gg t$ which corresponds to the realistic situation in manganites. The $H_{band} + H_{Kondo}$ part of the total Hamiltonian alone represents the DE mechanism and yields a FM ground state with $|x\rangle$ orbitals being occupied which is favored by the kinetic energy in 2D model. Such a fully spin polarized case at finite U leads to *the orbital t-J model* as considered in Refs. 43,44. Here, we are interested in the more complex case where both spin and orbital degrees of freedom play an active role. Therefore, an AF ($J_{AF} > 0$) coupling between nearest-neighbor t_{2g} spins is also incorporated,

$$H_{AF} = J_{AF} \sum_{\langle ij \rangle} \mathbf{S}_i \cdot \mathbf{S}_j. \quad (5)$$

In our numerical studies we assume $S = 1/2$ for the core spins which decreases the resulting Hilbert space considerably. We have tested that this assumption gives similar results as in the $S = 3/2$ case when J_H is renormalized⁴⁸ by the factor 3. Moreover, to promote the charge ordering as observed experimentally in half-doped manganites we include the Coulomb repulsion ($V > 0$) between e_g electrons on neighboring sites,⁴⁸

$$H_V = V \sum_{\langle ij \rangle \xi \zeta \sigma \sigma'} n_{i\xi\sigma} n_{j\zeta\sigma'}, \quad (6)$$

with $n_{i\xi\sigma} = \tilde{d}_{i\xi\sigma}^\dagger \tilde{d}_{i\xi\sigma}$. This term reduces the probability of occupancy of neighboring sites by e_g electrons.

The form of the inter-site OO interactions included in the H_{OO} term of the Hamiltonian will be specified in the following section.

B. Finite-temperature Lanczos method

To investigate the possible spin and orbital orderings in our spin-orbital model (1) we have calculated the temperature dependence of different two-site correlation functions given by the operator expectation value:

$$\langle A_{\mathbf{R}} \rangle = \frac{1}{Z} \sum_{n=1}^{N_{st}} \langle n | \exp(-\beta H) A_{\mathbf{R}} | n \rangle, \quad (7)$$

of two-site operators, $A_{\mathbf{R}} = 1/N \sum_{\mathbf{i}} B_{\mathbf{i}} B_{\mathbf{i}+\mathbf{R}}$ with $B_{\mathbf{i}} = n_{\mathbf{i}}$, $T_{\mathbf{i}}^z$, $S_{\mathbf{i}}^z$, or $S_{\mathbf{i}}^z n_{\mathbf{i}}$ with $n_{\mathbf{i}} = \sum_{\xi, \sigma} n_{i\xi\sigma}$.⁴⁸ Here, $\beta = 1/k_B T$, N_{st} is the number of basis states $\{|n\rangle\}$ that span H , N number of sites in the cluster and $Z = \sum_{n=1}^{N_{st}} \langle n | \exp(-\beta H) | n \rangle$ is the partition function.

The calculation of (7) would, however, require a complete diagonalization of a $N_{st} \times N_{st}$ matrix of the Hamiltonian. Therefore, we use for the calculation of $\langle A_{\mathbf{R}} \rangle$ a generalization of the exact diagonalization technique developed by Jaklič and Prelovšek.⁴⁹ In this approach

the trace of the thermodynamic expectation value is performed by a Monte Carlo sampling leading to the following approximate expression:

$$\langle A_{\mathbf{R}} \rangle \approx \frac{N_{st}}{LZ} \sum_{l=1}^L \sum_{j=1}^M \exp(-\beta E_j^l) \langle l | \psi_j^l \rangle \langle \psi_j^l | A_{\mathbf{R}} | l \rangle, \quad (8)$$

where the first sum is performed over a restricted number L of random states $|l\rangle$ being initial states in the Lanczos algorithm to generate a set $\{\psi_j^l\}$ of eigenfunctions of H with respective eigenvalues $\{E_j^l\}$. M is the number of Lanczos functions in the expansion of a given state $|l\rangle$. In the same manner the partition function is approximated by,

$$Z \approx \sum_{l=1}^L \sum_{j=1}^M \exp(-\beta E_j^l) |\langle l | \psi_j^l \rangle|^2. \quad (9)$$

It has been shown⁴⁹ that the results get very accurate already for $L, M \ll N_{st}$. Even though we exploit the translational symmetry the calculations are restricted to small clusters ($N = \sqrt{8} \times \sqrt{8}$ is used in this paper) as only $S_{tot}^z = \sum_{\mathbf{i}} S_{\mathbf{i}}^z$ subspaces can be treated separately, while a similar symmetry in the orbital sector does not exist. Although a $\sqrt{8} \times \sqrt{8}$ cluster is large enough to capture the CE-type correlations, boundary conditions can influence further neighbor interactions. To assess such finite size effects quantitatively, a full diagonalization on larger clusters would be necessary. In the case of the CO CE phase this would involve at least a 4×4 site cluster, which is far beyond numerical realization.

III. NUMERICAL RESULTS

A. Parameters and magnetic phases

In the numerical studies we assume $S = 1/2$ for the core spins and the limit of strong Hund's coupling $J_H/t = 15$. The numerical results are almost identical for all $J_H \gtrsim 5t$ in the whole range of temperatures considered by us. The Coulomb repulsion V/t and the AF-exchange J_{AF}/t are free parameters, and the data is summarized in form of a phase diagram in the $V - J_{AF}$ plane. The hopping parameter t is chosen as energy unit. We focus in this study on CO states and thus assume finite positive values for V in all the calculations. In perovskite manganites the effective hopping t strongly depends on the lattice parameters and distortions *e.g.* increases with contraction of the Mn–O bond length and also depends on the Mn–O–Mn bond angle.³ Thus, its value can be only roughly estimated as $t = 0.2 - 0.7$ eV.^{43,50,51,52}

A major difficulty when searching for spin structures like those indicated in Fig. 1, and the same applies to charge and orbital order, is that in a cluster with periodic boundary conditions translational (and rotational) symmetries are not broken. Therefore we have to investigate

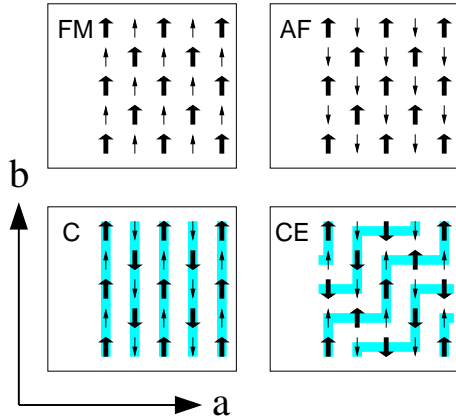


FIG. 1: Schematic view of different spin patterns found in the 2D model in presence of checkerboard CO (half-doped case). Thick (thin) arrows represent states with total spin $S = 2$ ($S = 3/2$) with (without) an e_g electron present at a given site, respectively. The shaded lines in C and CE phases indicate the direction of DE carrier propagation. The preferred directional e_g orbitals occupied at sites $S = 2$ are parallel to the shaded paths.

correlation functions and compare their features with the different spin configurations (presented in Fig. 1).

We shall consider three different forms for the orbital interaction term H_{OO} and show that one has to go beyond the nearest-neighbor interactions to obtain the CE-type correlations. We begin the description of our calculations with a simplified model (without H_{OO} term) but including the crystal-field splitting of e_g orbitals $\propto E_z$,

$$H_z = -E_z \sum_{\mathbf{i}} T_{\mathbf{i}}^z, \quad (10)$$

where $T_{\mathbf{i}}^z = \frac{1}{2} \sum_{\sigma} (n_{ix\sigma} - n_{iz\sigma})$ is the z component of the pseudospin operator. This orbital splitting accounts for the elongation of octahedra along the c -axis in layered compounds, which favors $|z\rangle$ over $|x\rangle$ orbital occupation, and also counterbalances the trend towards occupation of $|x\rangle$ orbitals, which is strongly favored by the kinetic energy in the 2D-model. Although, the model without H_{OO} interactions can lead to the stability of the CE-type orbital pattern,⁴⁸ the magnetic structure was FM. In a wide range of parameters ($E_z/t < 0$, $V/t > 0$, $J_{AF}/t > 0$) no stabilization of the AF CE spin phase was found, indicating that the inter-chain coupling is quite strong and cannot be neglected in realistic models for half-doped CO manganites. Such a conclusion agrees this recent density-functional calculations showing a considerable band dispersion normal to the chains.¹⁸ Thus, we argue that the *topological effect* considered in 1D model approximations, which gave a simple explanation of the existence of the CE spin-orbital phase at half-doping, is not likely to be the decisive mechanism in a more realistic 2D case investigated here. Our simulations with purely electronic interactions do not provide evidence for 1D FM chains that are coupled antiferromagnetically to neighbor

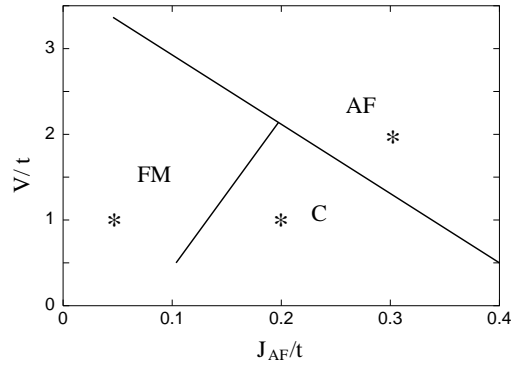


FIG. 2: Phase diagram indicating the character of the dominant spin correlations found at small temperatures $T < zJ$. The calculations include the nearest-neighbor OO effective interactions ($\kappa = 0.2t$). '*' indicates representative points for which the correlation functions are presented below.

chains, which is the basic assumption that could justify such 1D models. Therefore, in the following sections we concentrate on the electron-lattice coupling^{20,21,22,53,54} and present a mechanism stabilizing the CE spin/orbital state in manganites.

B. The role of nearest-neighbor orbital interactions

The first aim of our study of the spin-orbital model (1) in half-doped manganites is to investigate the role of nearest-neighbor OO coupling played in CO state. There are two different mechanisms contributing to this interaction: (i) the cooperative JT effect⁵² and (ii) superexchange interactions.^{43,55} Neglecting more complex spin-orbital terms^{51,52} both effects can be described by the following simple term derived before for undoped LaMnO₃ compound,⁵⁵

$$H_{OO} = 2\kappa \sum_{\langle ij \rangle} T_{ij}, \quad (11)$$

where the two-site orbital operator, T_{ij} , between nearest-neighbor Mn sites in the $\{|x\rangle, |z\rangle\}$ basis,

$$T_{ij} = T_i^z T_j^z + 3T_i^x T_j^x \mp \sqrt{3}(T_i^x T_j^z + T_i^z T_j^x), \quad (12)$$

is described in terms of pseudospin operators: $T_i^+ = \sum_{\sigma} \tilde{d}_{ix\sigma}^{\dagger} \tilde{d}_{iz\sigma}$, and $T_i^- = \sum_{\sigma} \tilde{d}_{iz\sigma}^{\dagger} \tilde{d}_{ix\sigma}$. The prefactor of the mixed term $\propto \sqrt{3}$ is negative in the a direction and positive in the b direction. The nearest-neighbor OO term can lead to *attraction* of electrons on neighboring sites with different orbital orientations but having the Coulomb repulsion (6) included in the model we avoid phase separation.

As shown in Fig. 2 for large values of the superexchange interaction between core spins ($zJ_{AF} \sim t$) an AF spin ground state is realized while with decreasing J_{AF} the

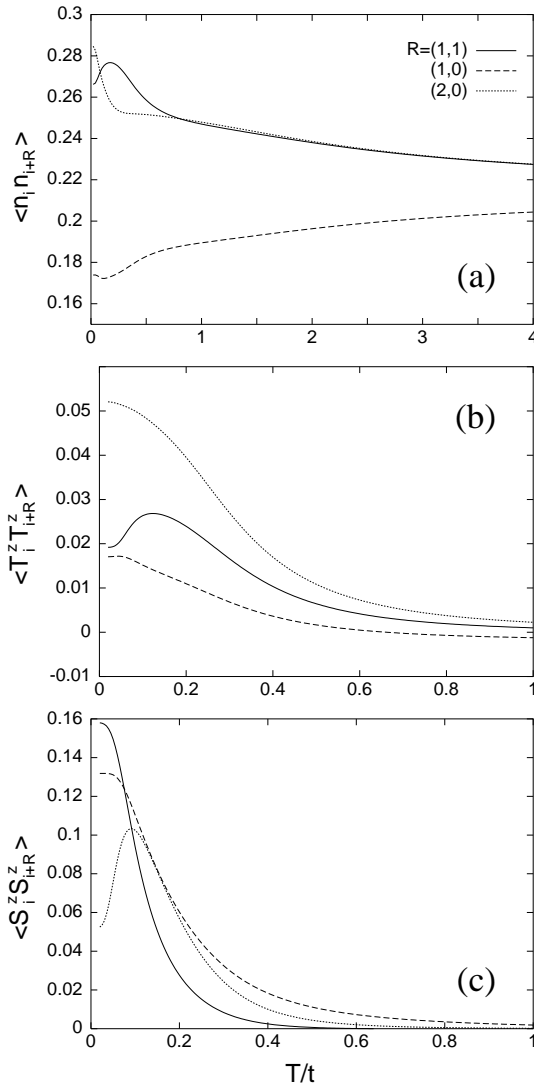


FIG. 3: Temperature dependence of the charge (a), orbital (b), and spin (c) two-site correlation functions calculated for neighbors at different distances \mathbf{R} for the phase with FM spin correlations. Parameters: $V = t$, $\kappa = 0.2t$, $J_{AF} = 0.05t$, $J_H = 15t$.

kinetic energy of the e_g electrons ($\sim t$) starts to play an active role via the DE mechanism³⁴ breaking some of the AF bonds which leads to 1D FM chains which form straight lines (C phase). Further decrease of J_{AF} yields FM correlations in both a and b directions. As the kinetic energy is controlled by the inter-site Coulomb repulsion V and suppressed in the limit of $V \gg t$ we find the AF region increasing in size with increasing V/t .

We discuss now in more detail the temperature dependence of the different correlation functions. Starting from the FM region (see Fig. 3) we find the evolution of weak CO for $T/t \lesssim 1$ with nearest-neighbor $(1,0)$ charge correlations smaller than the $(1,1)$ and $(2,0)$ next-neighbor ones which is consistent with the alternating order of Mn^{+3} and Mn^{+4} ions. The orbital corre-

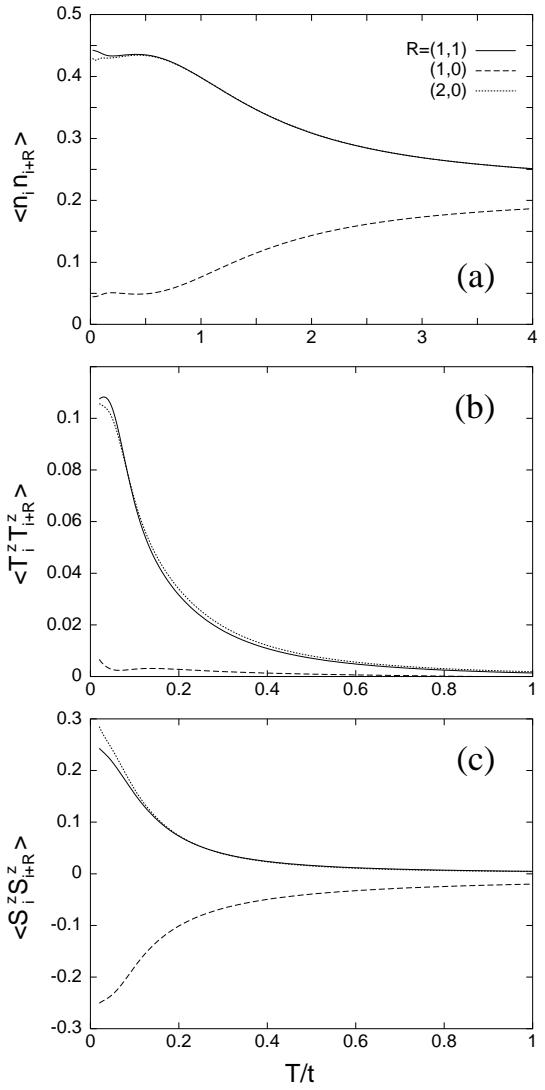


FIG. 4: Temperature dependence of the correlations as in Fig. 3 but for the phase with AF spin correlations. Parameters: $V = 2t$, $\kappa = 0.2t$, $J_{AF} = 0.3t$, $J_H = 15t$.

lations are positive between all neighbors indicating the preference of $x^2 - y^2$ orbital occupancy due to the kinetic energy which is quite large in the FM state. Although all spin correlation functions are positive, they remain highly anisotropic as $T \rightarrow 0$ as a result of the strong competition between the DE mechanism and AF superexchange interaction between core spins.

Next, we consider the AF spin state in the case of large J_{AF} and V (see Fig. 4). Increasing Coulomb repulsion ($V = 2t$) we find more distinct and almost isotropic alternation of the e_g charge which now sets in already at $T/t \approx 2$. Here, the orbital correlations are correlated with the onset of the AF spin order at $T/t \approx 0.5$. For $T/t \rightarrow 0$ the spin-spin correlations are strong and represent an almost isotropic AF spin state.

For intermediate values of J_{AF} and moderate Coulomb repulsion we find the phase with predominantly C spin

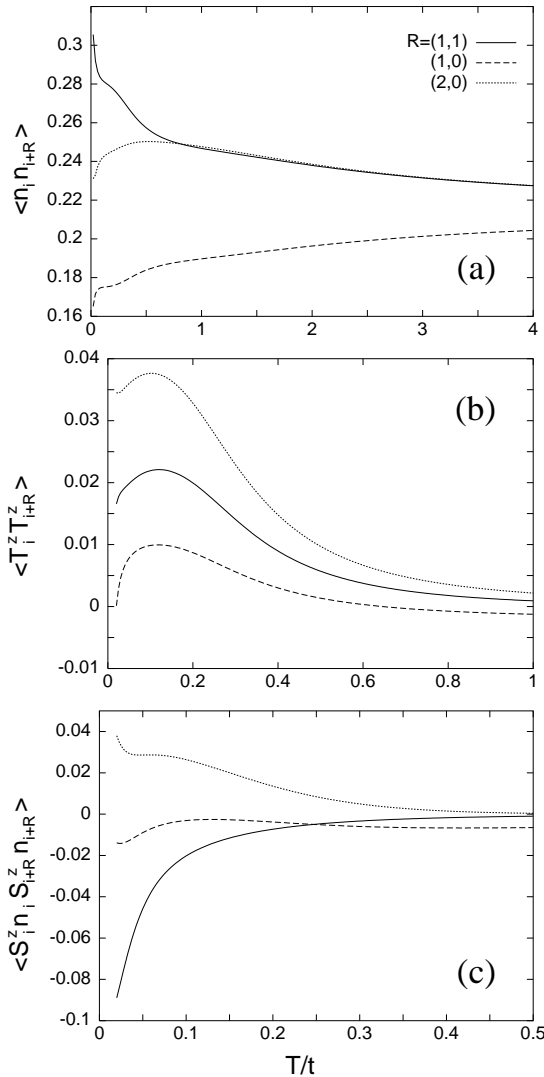


FIG. 5: Temperature dependence of the charge (a), orbital (b), and spin-charge (c) correlation functions calculated for the phase with C spin correlations. Parameters: $V = t$, $\kappa = 0.2t$, $J_{AF} = 0.2t$, $J_H = 15t$.

correlations at $T/t \rightarrow 0$ (see Fig. 2). As presented in Fig. 5 for $J_{AF}/t = 0.2$ and $V/t = 1$ the charge correlations are similar to those obtained for the FM state shown in Fig. 3 (a) while the spin ordering changes dramatically. Moreover for $T/t \rightarrow 0$ the orbital correlations are weaker than those found in the FM state discussed above indicating the orbital tendency towards in-plane directional-type order.

A convenient way to distinguish between phases with C or CE and other spin correlations is to evaluate a *combined spin-charge correlation function* being restricted to sites occupied by e_g electrons, $\langle S_i^z n_i S_{i+\mathbf{R}}^z n_{i+\mathbf{R}} \rangle$. Analyzing the localized limit presented in Fig. 1 (or its by $\pi/2$ rotated version) one can easily see that, for the C phase one should find $\langle S_i^z n_i S_{i+\mathbf{R}}^z n_{i+\mathbf{R}} \rangle > 0$ for $|\mathbf{R}| = 2$ and $\langle S_i^z n_i S_{i+\mathbf{R}}^z n_{i+\mathbf{R}} \rangle < 0$ for $|\mathbf{R}| = \sqrt{2}$ while for the

CE phase only $\langle S_i^z n_i S_{i+\mathbf{R}}^z n_{i+\mathbf{R}} \rangle < 0$ for $|\mathbf{R}| = 2$ with any other spin-charge correlations remaining small. In the case presented in Fig. 5 $\langle S_i^z n_i S_{i+\mathbf{R}}^z n_{i+\mathbf{R}} \rangle$ functions are negative (positive) for nearest-neighbors along diagonal (next-nearest-neighbors along a/b direction), respectively, in agreement with the arguments presented above. Furthermore, nearest-neighbor spin-charge correlations are small as a result of averaging over different cluster orientations (rotated by angles $\pm\pi/2$, $\pm\pi$).

It is straightforward to see why the C-structure is favored by the nearest-neighbor JT interaction. The C-phase can be viewed as a realization of the alternating orbital structure of LaMnO_3 but with a modulated charge density. Hence this structure is compatible with the nearest-neighbor JT interaction, whereas in the CE-structure this interaction is frustrated.

C. Elastic interactions

The role of local lattice distortions due to the JT effect, which creates an anisotropic strain field decaying as $\sim R^{-3}$ and thereby promotes long-range orbital ordering, was considered by Khomskii (see Ref. 41). Following these arguments, we treat the OO term as an elastic interaction which is active also between e_g electrons on next-nearest-neighbor sites along a or b direction,

$$H_{el} = 2\kappa \sum_{\langle ij \rangle} T_{ij} + 2\kappa' \sum_{\langle \langle ij \rangle \rangle} T_{ij}, \quad (13)$$

where $\langle \langle ij \rangle \rangle$ refers to next nearest-neighbors along a and b direction with $\kappa' = \kappa/8$ which follows from the $\sim (|i-j|)^{-3}$ decay of elastic interactions.⁴¹ The existence of longer-range OO interactions is justified by its cooperative lattice-driven nature where an orbital flip on a single Mn site distorts not only the neighboring oxygens but also positions of other manganese ions around it. Here, the JT coupling preferring the tilting of the orbitals from the uniform orbital state leads to an alternating orbital order (see Fig. 6) and in this way compensates for the kinetic energy gain in uniform $|x\rangle$ orbital state favored in the 2D model. Here we neglect non-central elastic interactions between neighboring Mn sites in (11) direction as their strength does not scale with κ' (see Ref. 41) and thus would involve introduction of an additional parameter in the model.

The CE phase is favored as compared to the C phase by the OO coupling between second neighbors ($\sim \kappa'$) along a/b direction. However, this interaction is only active (not screened) when strong charge ordering takes place (large V/t case) and here the CE phase can persist even for small values of J_{AF} as long as the e_g kinetic energy is sufficiently suppressed by a large V (see Fig. 7). Thus, one has to assume large inter-site Coulomb repulsion (where almost perfect $\text{Mn}^{+3}/\text{Mn}^{+4}$ charge ordering⁶ is realized) and small superexchange interaction [see an example for $V/t = 3$ and $J_{AF}/t = 0.04$ in Fig. 8]. In

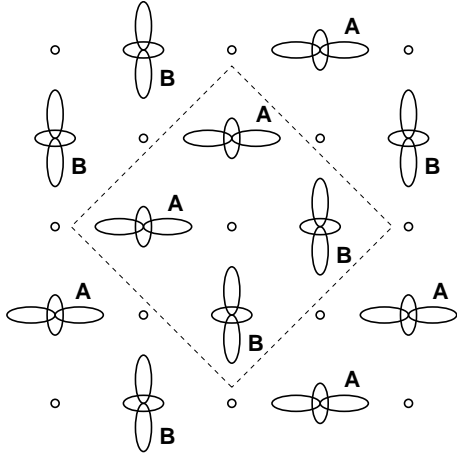


FIG. 6: Schematic configuration of the charge-orbital ordered CE phase. The sites **A** and **B** indicate two orbital Mn^{3+} sublattices while empty circles stand for the Mn^{4+} ions. The dashed-line box indicates a typical orbitals orientation around a given Mn^{4+} ion.

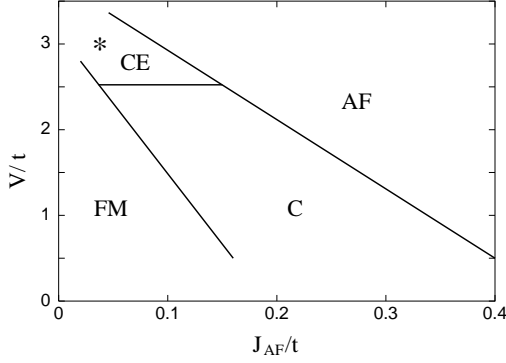


FIG. 7: Phase diagram as in Fig. 2 including the nearest- and next-neighbor elastic interactions ($\kappa = 0.2t$, $\kappa' = \kappa/8$). '*' indicates a representative point in the CE region for which the correlation functions are presented here.

the $\{|x\rangle, |z\rangle\}$ basis, which we use in most of the numerical evaluations, the spin and orbital correlation functions with $\mathbf{R} = (2, 0)$ become large as $T \rightarrow 0$ while all the others remain very small in the whole range of temperatures. Such small orbital correlations imply either that the respective orbitals are uncorrelated or that they order in such a way, that the occupied orbitals are linear combinations with almost equal amplitude expressed in the basis used for the measurement of correlation functions.⁴³ This difficulty is not present in SU(2) symmetric models, and appears here as consequence of the cubic symmetry in the orbital sector. Therefore, the same functions were evaluated also in the $\{(|x\rangle \pm |z\rangle)/\sqrt{2}\}$ basis as presented in the inset of Fig. 8 (b). In the new orbital basis the function $\langle T_i^z T_{i+(2,0)}^z \rangle$ is more pronounced and saturates for $T/t \simeq 0.1$ at $\langle T_i^z T_{i+(2,0)}^z \rangle \simeq -0.12$ close to its maximum value $-1/8$ indicating almost perfect CE

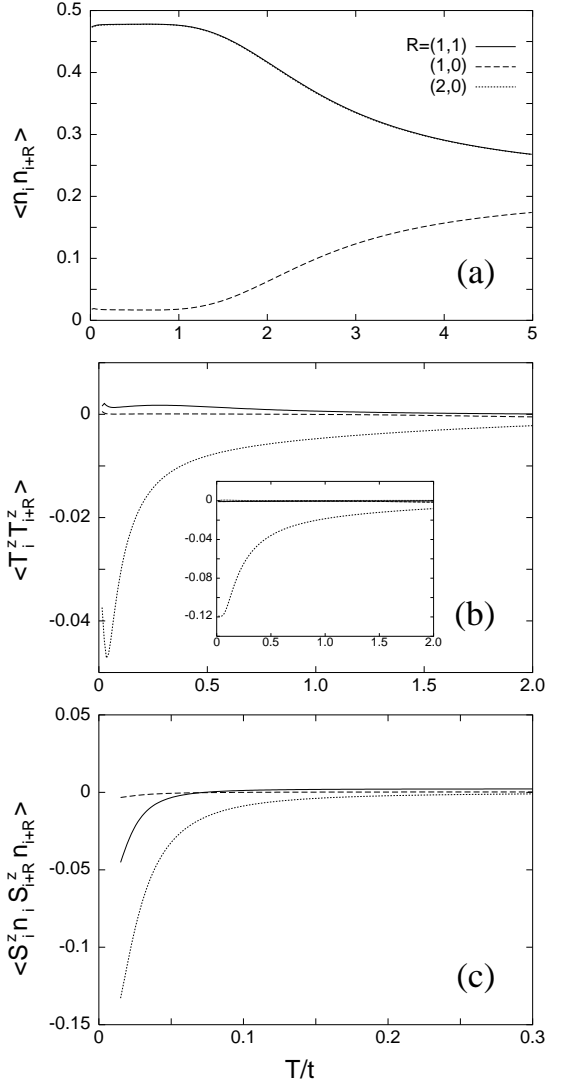


FIG. 8: Temperature dependence of the two-site correlations as in Fig. 5 but for the phase with CE spin and orbital correlations promoted by elastic interactions ($\kappa = 0.2t$, $\kappa' = \kappa/8$). Other parameters: $V = 3t$, $J_{AF} = 0.04t$, $J_H = 15t$. The inset in (b) shows the orbital correlations in the rotated basis: $\{(|x\rangle \pm |z\rangle)/\sqrt{2}\}$.

orbital structure (see Fig. 6). Shorter range $\langle T_i^z T_{i+R}^z \rangle$ correlations should become small when averaged over differently oriented clusters (rotated by angles $\pm\pi/2$) [see Fig. 1 (d)]. From Fig. 1 (d) one can see that a similar pattern as found for the two-site orbital correlations should be found for the $\langle S_i^z n_i S_{i+R}^z n_{i+R} \rangle$ functions. In our cluster in ideal CE state only electrons at distance $|\mathbf{R}| = 2$ can contribute to the charge-spin correlations (being negative in this case) which do not vanish when averaged over different cluster orientations. As shown in Fig. 8 (c) the $\langle S_i^z n_i S_{i+R}^z n_{i+R} \rangle$ correlations obtained here are consistent with the above characterization of the CE pattern with a strong negative signal dominating at distance $|\mathbf{R}| = 2$. The existence of charge-ordered insulating

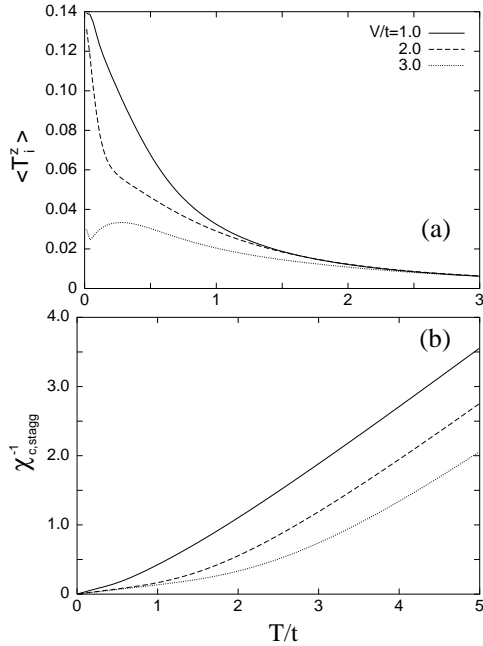


FIG. 9: Temperature dependence of the average value of the T_i^z orbital operator (a) and the inverse of the staggered charge susceptibility $\chi_{c,stagg}^{-1}$ (b) obtained for different values of the inter-site repulsion V/t in the presence of elastic interactions ($\kappa = 0.2t$, $\kappa' = \kappa/8$). Other parameters: $J_{AF} = 0.04t$, $J_H = 15t$.

state concomitant with orbital and spin order of the CE-type^{8,9} was observed in different half-doped manganites with small one-electron bandwidth.¹

The average change in the orbital occupation can be studied calculating $\langle T_i^z \rangle$ which changes between $+1/4$ and $-1/4$ for the uniform $|x\rangle$ and $|z\rangle$ orbital states, respectively, for the case with one e_g electron per two Mn sites. Furthermore, when the orbital state involves $|x\rangle$ and $|z\rangle$ orbitals in the same proportion one finds $\langle T_i^z \rangle \simeq 0$. In Fig. 9 (a) we see that increasing the Coulomb interaction from $V = t$ to $V = 2t$ the orbital ordering hardly changes for $T/t \rightarrow 0$ with $\langle T_i^z \rangle$ only slightly decreasing to $\langle T_i^z \rangle \simeq 0.13$ for $V = 2t$. This indicates that as long as the system is in the FM state (see Fig. 7) the ground state is dominated by the $x^2 - y^2$ orbital promoted by the kinetic energy term. Further increase in the Coulomb inter-site repulsion to $V = 3t$ leads to a drastic change in the orbital order when system enters the CE phase region (see Fig. 7). Here, $\langle T_i^z \rangle \simeq 0.03$ for $T/t \rightarrow 0$ indicating dominating role played by the $(|x\rangle \pm |z\rangle)/\sqrt{2}$ orbitals. This fact is consistent with our results for the two-site orbital correlation functions [see inset in Fig. 8(b)].

A change in the inter-site Coulomb interaction is directly connected with the robustness of the charge ordering as seen in Figs. 3 - 5 (a) and Fig. 8 (a). Although the characteristic temperature of the CO (T_{CO}) can be roughly estimated from the charge-charge correlation functions it can be more precisely extracted from

the staggered charge susceptibility,⁴⁸ $\chi_{c,stagg}$:

$$\chi_{c,stagg} = \beta/N \sum_{ij} (-1)^{|i-j|} \left(n_i - \frac{1}{2} \right) \left(n_j - \frac{1}{2} \right), \quad (14)$$

which at high temperatures follows a Curie-Weiss law $\chi_{c,stagg}^{-1} \propto (T - T_{CO})$. From Fig. 9 (b) one can easily estimate $T_{CO}/t \approx 0.6, 1.4$, and 2.4 for $V/t = 1.0, 2.0$, and 3.0 , respectively, in agreement with the mean-field solution⁵⁶ which for $V \gg t$ predicts, $T_{CO} \approx zV/4$.

D. Microscopic model for Mn^{3+} - Mn^{3+} JT coupling

Although the model considered in the previous section with longer-range OO elastic coupling leads to the CE-type spin and orbital correlations, this phase is found only in a very extreme case of almost perfect Mn^{4+}/Mn^{3+} CO (that is for strong Coulomb repulsion) which may not be very realistic in the light of some experimental facts indicating the CDW character of charge redistribution between different manganese ions.³³ Therefore in this section we derive the further neighbor OO interactions from a microscopic model including apart from the JT-distortion of the Mn^{3+} octahedra the breathing distortion around the Mn^{4+} ions as well. We then show that this interaction is capable to produce the zigzag (spin and orbital) phase in a region of small Coulomb repulsion changing the previous phase diagrams in a drastic way.

To assess the gain in lattice energy connected with the formation of the CE long-range orbital order we follow the work of Millis for $LaMnO_3$ by treating the lattice distortions classically.^{57,58} The effect of lattice displacements is described by assuming arbitrary values of four different lattice distances d_i ($i = 1, \dots, 4$) (see Fig. 10) which are expressed by δ_x , δ'_x – uniform deformation along the a and b direction of the Mn lattice, and u_i – displacements of O ions along the Mn–O–Mn bonds within the (a, b) planes:

$$d_1 = \frac{1}{2}b(1 + \delta_x - 2u_1), \quad (15a)$$

$$d_2 = \frac{1}{2}b(1 + \delta_x + 2u_1), \quad (15b)$$

$$d_3 = \frac{1}{2}b(1 + \delta'_x + 2u_2), \quad (15c)$$

$$d_4 = \frac{1}{2}b(1 + \delta'_x - 2u_2), \quad (15d)$$

where b is the lattice constant of the ideal perovskite.⁵⁹ Moreover, we assume e_g charge stacking in the c direction with the respective Mn–Mn distance being $b(1 + \delta_z)$.

In order to define orbital sublattices (A and B) we introduce a transformation which describes the tilting of orbitals by making two different transformations at both sublattices,⁵⁵

$$\begin{bmatrix} |i\mu\rangle \\ |i\nu\rangle \end{bmatrix} = \begin{bmatrix} \cos\left(\frac{\pi}{4} \pm \phi\right) & \sin\left(\frac{\pi}{4} \pm \phi\right) \\ -\sin\left(\frac{\pi}{4} \pm \phi\right) & \cos\left(\frac{\pi}{4} \pm \phi\right) \end{bmatrix} \begin{bmatrix} |iz\rangle \\ |ix\rangle \end{bmatrix}, \quad (16)$$

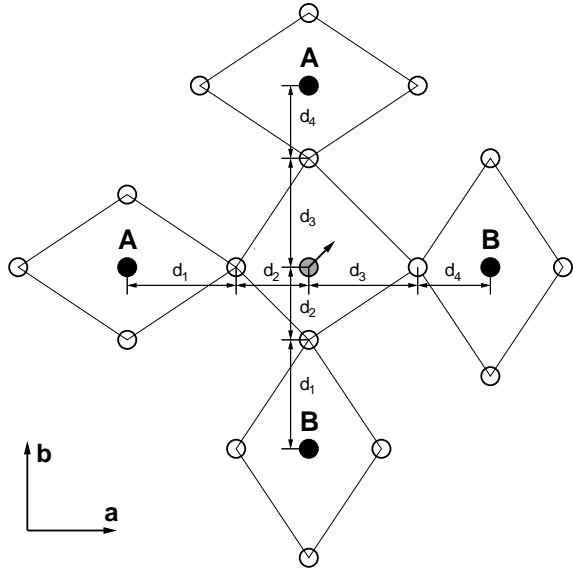


FIG. 10: Schematic representation of the lattice distortions contributing to the second neighbor JT-interaction. The corresponding CE orbital order for the 5 atom structure above is indicated in Fig. 6 by dashed lines. Different Mn^{3+} , Mn^{4+} , and O ions are presented by full, shaded and empty circles, respectively. The distances between the Mn^{4+} ion and the Mn^{3+} ions in (10) [$(\bar{1}0)$] and (01) [$(0\bar{1})$] directions, respectively, are identical. The arrow indicates the displacement of the central Mn^{4+} ion when $d_1 + d_2 \neq d_3 + d_4$.

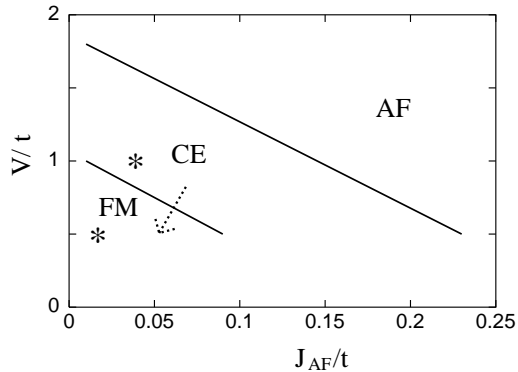


FIG. 11: Phase diagram as in Fig. 2 including the local nearest- and next-neighbor OO interactions with $\kappa = 0.2t$ and $\kappa' = 0.1t$ (spring constants $K_2/K_1 = 0.25$). '*' indicate representative points in the CE region for which the correlation functions are presented here. The dashed arrow presents the direction of the transition from the localized CE to the itinerant electron A-phase at low temperatures.

where $-$ ($+$) refers to $i \in A$ ($i \in B$) sublattice, respectively, and $|\phi| \leq \frac{\pi}{4}$. Here, $|ix\rangle$ and $|iz\rangle$ stands for local basis orbitals: $|x\rangle$ and $|z\rangle$ at site i , respectively. In the rotated basis $\{|i\mu\rangle, |i\nu\rangle\}$ we assume for the transformed operators: $\langle T_i^z \rangle = -1/2$ ($1/2$) for $i \in A$ (B) sublattice, respectively. At intermediate values of ϕ one can reach, e.g., $|3x^2 - r^2\rangle/|3y^2 - r^2\rangle$ ($|z^2 - x^2\rangle/|z^2 - y^2\rangle$)-type orbital

ordering at $\phi = \pi/12$ ($\phi = -\pi/12$), respectively. The rotation (16) does not include complex orbital order which was proposed as a possible orbital order in manganites at smaller doping.⁶⁰ The classical energy of the distorted lattice E_l (per Mn site) is given by,⁵⁸

$$E_l = \frac{1}{4} (K_1 + 2K_2) [\delta_x^2 + (\delta'_x)^2 + \delta_z^2] + K_1 (u_1^2 + u_2^2), \quad (17)$$

normalized per Mn ion, where K_1 (K_2) are the nearest-neighbor Mn–O (Mn–Mn) spring constant, respectively. Here the force constants include the factor b^2 , and hence have the dimension of an energy.

Next, we have to add the energy of the breathing mode (BM) describing the attraction between oxygen ions and the unoccupied Mn^{+4} site:

$$E_{br} = \frac{1}{2} \beta \lambda (\delta_x + \delta'_x + \delta_z + u_1 + u_2). \quad (18)$$

Here, all oxygens are equally attracted towards the central manganese ion. The BM induces charge alternation on neighboring Mn sites and contributes to the effective inter-site charge-charge repulsion (V). The coupling constant to the breathing distortion is written as $\beta\lambda$, where λ denotes the coupling to the JT distortion. The term describing the JT coupling depends on the character of the occupied orbital at a Mn^{+3} site. The JT interaction describes the coupling between the occupied e_g orbital at a particular Mn^{3+} ion and the distortions of the surrounding oxygen ions, as introduced by Millis.⁵⁷ In the orbitally rotated state (16) this energy has the following form,

$$E_{JT}(\phi) = \frac{1}{2} \lambda \left\{ \left[\delta_z + u_1 + u_2 - \frac{1}{2} (\delta_x + \delta'_x) \right] \sin(2\phi) - \sqrt{3} \cos(2\phi) \left[\frac{1}{2} (\delta_x - \delta'_x) + u_2 - u_1 \right] \right\}, \quad (19)$$

and depends on the rotation angle ϕ and on the deformation of the lattice.

The optimal values of the ionic displacements for a given angle ϕ are found by minimization of the total energy, $E_{tot}(\phi) = E_l + E_{br} + E_{JT}(\phi)$, which for (17)–(19) and neglecting higher-order nonlinear terms gives,

$$\delta_x = \frac{-\lambda [2\beta - \sin(2\phi) - \sqrt{3} \cos(2\phi)]}{2(K_1 + 2K_2)}, \quad (20a)$$

$$\delta'_x = \frac{-\lambda [2\beta - \sin(2\phi) + \sqrt{3} \cos(2\phi)]}{2(K_1 + 2K_2)}, \quad (20b)$$

$$\delta_z = \frac{-\lambda [\beta + \sin(2\phi)]}{K_1 + 2K_2}, \quad (20c)$$

$$u_1 = \frac{-\lambda [2\beta + \sin(2\phi) + \sqrt{3} \cos(2\phi)]}{4K_1}, \quad (20d)$$

$$u_2 = \frac{-\lambda [2\beta + \sin(2\phi) - \sqrt{3} \cos(2\phi)]}{4K_1}. \quad (20e)$$

This yields for the total energy of the distorted lattice,

$$E_{tot}(\phi) = -\frac{\lambda^2}{4K_1(K_1 + 2K_2)} \{ \beta^2(5K_1 + 4K_2) + (K_1 + 2K_2)[2\beta \sin(2\phi) + \cos^2(2\phi)] + 2K_1 + K_2 \}. \quad (21)$$

This implies a change of the volume of the lattice with respect to the ideal perovskite ($V_0 = b^3$) $\delta V/V_0 \simeq \delta_x + \delta'_x + \delta_z = -3\lambda\beta/(K_1 + 2K_2)$. Hence the volume decreases with increasing BM coupling β , but does not depend on the character of the orbital order.

The relative strength of the effective next- and nearest-neighbor JT interactions can be obtained by comparing the lattice stiffnesses of the orbital modulations in the undoped ($\sim \kappa$) and the quarter-filled ($\sim \kappa'$) case, respectively. For *undoped* LaMnO₃ the lattice energy was found to be [see Eq. (2.14) in Ref. 61],

$$E_{tot}^0(\phi) = -\frac{3\lambda^2}{K_1(K_1 + 2K_2)} \{ K_1 + K_2 [1 + \cos(4\phi)] \}, \quad (22)$$

In the half-doped case the orbital alternation at Mn³⁺ neighbors is driven by the Mn⁴⁺ ion shift. The energy (21) can be decomposed $E_{tot}(\phi) = E_0(\phi) + \delta E(\phi)$, where $\delta E(\phi)$ is the gain of energy due to the Mn⁴⁺ displacement:

$$\delta E(\phi) = -\frac{3\lambda^2}{16(K_1 + 2K_2)} [1 + \cos(4\phi)]. \quad (23)$$

This cooperative energy does not depend on the breathing mode coupling β directly, though there is an indirect dependence via $E_0(\phi)$ influencing the optimal value for ϕ . Contrary to the undoped case (22), where the Mn-Mn potential ($\sim K_2$) is necessary to obtain finite orbital stiffness, in the half-doped case (23) the Mn-O interaction alone can lead to cooperative JT effect stabilizing the alternating orbital order. Assuming $\lambda = 6\text{eV}$, $K_1 = 200\text{ eV}$, and $0 < K_2/K_1 < 1$ (see Ref. 57,62) one finds for the $|\langle x \rangle \pm \langle z \rangle|$ ($\phi = 0$) orbital order the CE energy contribution per Mn ion $\delta E \simeq 20 - 70\text{ meV}$.

In Table I we present the ratio $\delta E(\phi)/E_{tot}(\phi)$, characterizing the stability of the CE orbital order, as function of the BM coupling strength β and the ratio of spring constants K_2/K_1 . The largest relative gain in energy due to the Mn⁴⁺ ions shift ($\sim |\delta_x - \delta'_x|b/2$) is obtained for the $(|\langle x \rangle + \langle z \rangle|)/(|\langle x \rangle - \langle z \rangle|)$ orbital order ($\phi = 0$) which for small BM coupling ($\sim \beta$) can reach up to 50% of the total lattice energy, whereas for larger values of β , although $\delta E(\phi)$ is not changed, the total lattice energy increases rapidly as $\sim \beta^2$ being dominated by the distortions of the MnO₆ octahedra rather than by their displacements. Furthermore, with increasing Mn lattice stiffness ($\sim K_2/K_1$) both the $\delta E(\phi)/E_{tot}(\phi)$ ratio and the shift of unoccupied Mn⁴⁺ ions [$\sim \lambda/(K_1 + 2K_2)$] decrease.

Comparing the cooperative part [$\sim \cos(4\phi)$] of both JT energy contributions [(22) and (23)] we end up

TABLE I: The relative energy gain, $\delta E(\phi)/E_{tot}(\phi)$, associated with the Mn⁴⁺ ion displacement (see Fig. 10) for the orbital orderings given by $\phi = 0$ and $\pm\pi/12$ presented as function of β and K_2/K_1 .

β	K_2/K_1	$\phi = \pi/12$		$\phi = 0$		$\phi = -\pi/12$	
		$\delta E(\phi)/E_{tot}(\phi)$					
0.0	0.0	0.409		0.500		0.409	
0.5	0.0	0.321		0.353		0.250	
1.0	0.0	0.167		0.187		0.129	
0.0	0.5	0.281		0.333		0.281	
0.5	0.5	0.237		0.240		0.167	
1.0	0.5	0.125		0.130		0.087	
0.0	1.0	0.214		0.250		0.214	
0.5	1.0	0.187		0.182		0.125	
1.0	1.0	0.100		0.100		0.065	

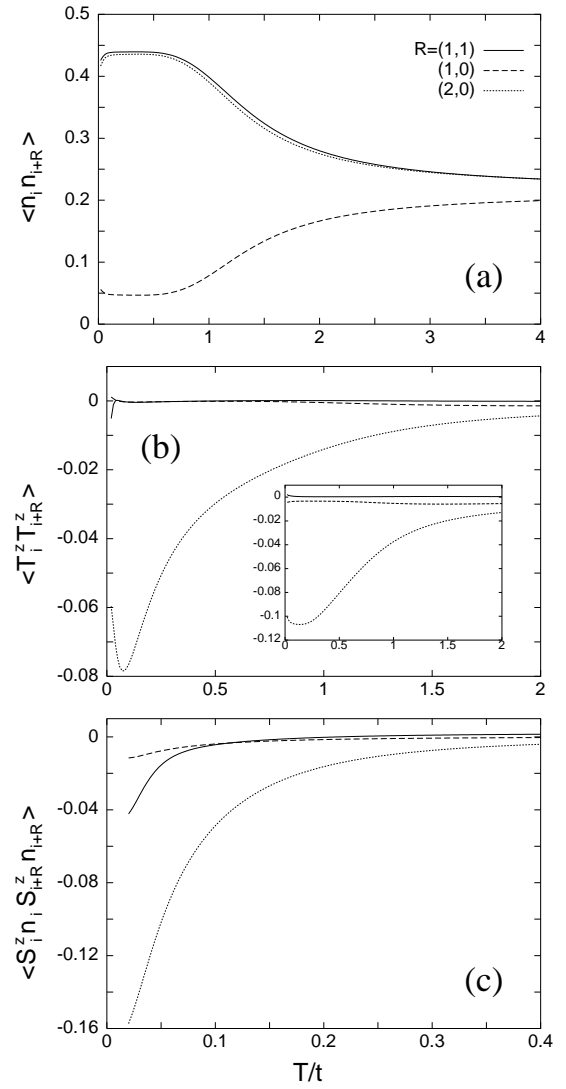


FIG. 12: Correlation functions in the case of a CE ground state (as in Fig. 8) but obtained for the local OO interaction (26) with spring constants $K_2/K_1 = 0.25$ ($\kappa' = \kappa/2$). Other parameters: $V = t$, $\kappa = 0.2t$, $J_{AF} = 0.04t$, $J_H = 15t$.

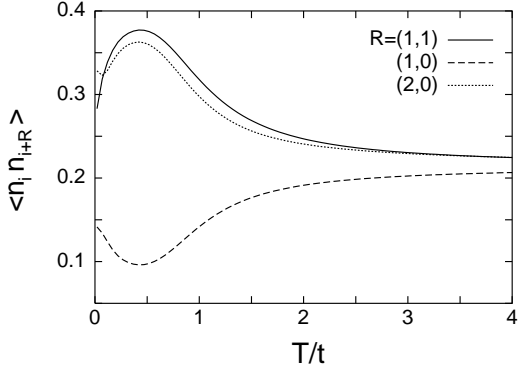


FIG. 13: Charge correlations in the case of a FM ground state as obtained for the local OO interaction with spring constants $K_2/K_1 = 0.25$ ($\kappa' = \kappa/2$). Other parameters: $V = 0.5t$, $\kappa = 0.2t$, $J_{\text{AF}} = 0.02t$, $J_H = 15t$.

with a simple relation between different OO interaction strengths,

$$\frac{\kappa'}{\kappa} = \frac{K_1}{8K_2}. \quad (24)$$

For $K_2 = K_1$ the $\sim R^{-3}$ scaling of elastic interactions⁴¹ is recovered. In the above estimate we have neglected the superexchange interaction which can also contribute to the effective κ [see *e.g.* Eq. (2.7) in Ref. 61].

The relative strength of both spring constants in the CO case can be assessed from the relative length of different bonds in the half-doped MnO_2 plane. As measured for low-temperature $\text{La}_{0.5}\text{Ca}_{0.5}\text{MnO}_3$ superstructure⁴⁰ the length of all four in-plane Mn^{4+} -O bonds is very similar ($d_2 = d_3 \simeq 1.915\text{\AA}$). Neglecting the effect of Mn-O-Mn bond bending and assuming $d_2 \simeq d_3$ (see Fig. 10) one obtains the relation,

$$K_2 \ll K_1, \quad (25)$$

by using Eqs. (20). The above assessment together with (24) underlines the importance of Mn^{3+} - Mn^{3+} orbital coupling ($\sim \kappa'$) in CO manganites.

The structural data of Radaelli *et al.*⁴⁰ may be used in combination with Eqs. (20 a-e) to infer the values for λ and β . We have not attempted to determine the force constants as well, but assume⁵⁷ $K_1 = 200$ eV. Using basically data for the JT-distortion of Mn^{3+} -O in-plane bonds ($d_1 \simeq 2.07\text{\AA}$ and $d_4 \simeq 1.92\text{\AA}$) and the Mn^{4+} displacement, we obtain for $K_2 = 0.25(0.0)K_1$ $\beta \simeq 0.27(0.35)$ and $\lambda \simeq 7.4(5.7)$ eV, respectively. We note that the ratio $\lambda/K_1 \simeq 0.037(0.029)$ is rather close to the values determined by Millis⁵⁷ for LaMnO_3 . This also implies that the energy gain due to the breathing distortion is substantial [see Eq. (21)].

E. Effect of cooperative Mn^{3+} - Mn^{3+} JT interactions

We return to the many-body theory for a translation invariant system. As the OO interaction between further Mn^{3+} neighbors is mediated by an Mn^{4+} ion we introduce the following effective three-site interaction,

$$H'_{\text{OO}} = 2\kappa' \sum_{\langle \mathbf{ij}' \rangle} (1 - n_{\mathbf{j}}) T_{\mathbf{ij}'}, \quad (26)$$

where the operator $T_{\mathbf{ij}'}$ is defined as in Eq. (12), and $\langle \mathbf{ij}' \rangle$ denotes three neighboring sites along a or b direction. The reasoning here is similar as for the nearest-neighbor JT interaction in Eq. (11), i.e., the expectation value of the operator $T_{\mathbf{ij}'}$ in an orbital ordered state depends on the orbital angle precisely as in Eq. (23), namely $\sim [1 + \cos(4\phi)]$. The $(1 - n_{\mathbf{j}})$ factor in Eq. (26) reflects the charge state of Mn^{4+} and favors CO in the quarter-filled system, while the contribution of the interaction (26) would vanish in the undoped compound.

Investigating the model (1) with both nearest-neighbor (11) and three-site (26) OO couplings we find a strong change in the low-temperature phase diagram (see Fig. 11) as compared with the previous ones (Figs. 2 and 7). Assuming $\kappa' = \kappa/2$ (which corresponds to $K_2/K_1 = 1/4$), the CE-like correlations set in already at rather small inter-site repulsion ($V \simeq 0.5t$) while for stronger Coulomb interactions ($V \gtrsim 1.5t$) the spin correlations have predominantly AF character. Furthermore, the FM region is quite small and can be found only for $V \lesssim t$ and $J_{\text{AF}} \lesssim 0.1t$. When decreasing the ratio K_2/K_1 (and keeping the value of κ' constant) the FM region shrinks at the expense of the CE region.

Next, we present the two-site correlations for one representative ($V = t$, $J_{\text{AF}} = 0.04t$) point in the CE region in Fig. 11. From Fig. 12 (a) one sees that the CE state can exist for less pronounced CO than in the elastic strain model considered in Sec. III C, where almost perfect Mn^{3+} / Mn^{4+} CO was necessary to stabilize the zigzag state (see Fig. 8). Moreover, the evolution of CE-type orbital order with decreasing temperature is here correlated with the onset of CO [compare Fig. 12 (a)-(b) with 8 (a)-(b)]. Regarding $\langle S_i^z n_i S_{i+R}^z n_{i+R} \rangle$ correlations, the CE-type spin order develops at lower temperatures than the charge and orbital order but at higher temperature than previously found for the strain induced interactions. The three-site term (26) which is active for a Mn^{3+} - Mn^{4+} - Mn^{3+} sequence along the a and b direction, respectively, promotes not only orbital alternation on neighboring Mn^{3+} sites but also strengthens CO. This is clearly seen in the charge correlations which are now stronger than those *e.g.* in Fig. 3, although the same Coulomb repulsion ($V = t$) was assumed in both cases.

Going from the CE to the FM phase (as indicated by an arrow in Fig. 11) one finds that the CDW is now reduced at low temperatures in the FM state (Fig. 13), while the charge modulation is still rather strong at higher temperatures ($T/t \approx 0.5$) above the Néel temperature where the

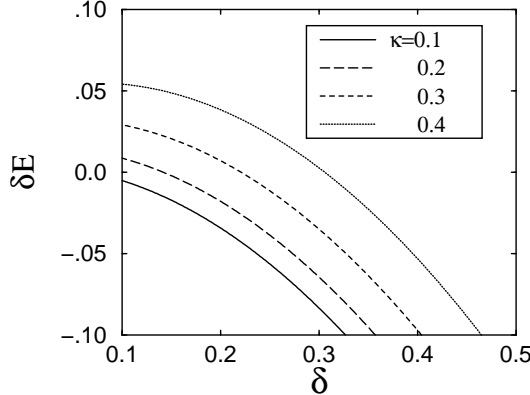


FIG. 14: Energy gained by e_g electron stacked in the c direction as function of charge modulation δ obtained for $V = 0.5t$, $\kappa' = 0.1t$ and different values of κ .

electron kinetic energy is quenched due to the random t_{2g} spin orientations. This behavior is a clear manifestation of the DE mechanism. We note that the CE-type orbital correlations are still present in the FM phase in Fig. 11 for $V \gtrsim 0.5t$, whereas for smaller values for V x^2-y^2 orbital correlations dominate, which are characteristic for the metallic A-phase.

F. Charge modulation in the c direction

Finally, we consider possible mechanisms stabilizing the charge stacking of CE-ordered planes⁶⁵ as observed in most charge-ordered manganites at doping $x = 1/2$. Any interaction stabilizing such a stacking must overcome the inter-site charge-charge repulsion. There are two interactions which contribute to such a repulsion: (i) the electron-electron Coulomb force V ; and (ii) the BM coupling. Both interactions will effectively tend to maximize the number of $\text{Mn}^{3+}-\text{Mn}^{4+}$ bonds. The BM coupling contribution to the inter-site charge-charge repulsion (V_{BM}) can be estimated comparing the lattice energies with charge alternating and stacked along the c direction which leads to the estimate $V_{\text{BM}} = \lambda^2[\beta - \sin(2\phi)]^2/(2K_1)$. Assuming typical values for $\lambda = 10t$ and $K_1 = 500t$ (see Ref. 57) together with our previous estimate $\beta \simeq 0.35$ one can obtain *e.g.* $V_{\text{BM}} \simeq 0.012t$ for the $\{(|x\rangle \pm |z\rangle)/\sqrt{2}\}$ CE orbital order.

In a multi-layer system the OO interaction along the c direction is given by the nearest-neighbor coupling $\sim \kappa$, which in the $\{(|x\rangle, |z\rangle)\}$ basis has the form,⁵⁵

$$H_{\text{OO}}^c = 8\kappa \sum_{\langle ij \rangle c} T_i^z T_j^z. \quad (27)$$

This interaction together with the $\sim \kappa'$ coupling, which controls the CE-orbital order in the (a, b) plane, in a charge-ordered case yields an approximate orbital model

of the form,

$$H_{\text{OO}} \simeq 6\kappa' \sum_{\langle ij \rangle ab} T_i^z T_j^z + 8\kappa \sum_{\langle ij \rangle c} T_i^x T_j^x. \quad (28)$$

where T_i^z (T_i^x) are defined with respect to the $\{(|x\rangle \pm |z\rangle)/\sqrt{2}\}$ orbital basis. Defining $|\pm\rangle \equiv (|x\rangle \pm |z\rangle)/\sqrt{2}$ and assuming that in the (a, b) planes of a bilayer system $|+\rangle_i$ and $|+\rangle_j$ orbitals are occupied on two neighboring sites in the c direction, the $\sim \kappa$ coupling [see Eq. (28)] rotates orbitals towards the $|-\rangle_i \otimes |-\rangle_j$ configuration and leads to binding of two electrons with energy $E_b = \sqrt{(12\kappa')^2 + 4\kappa^2} - 12\kappa'$. For charge disproportion with $\text{Mn}^{3.5\pm\delta}$ ions alternating in the (a, b) planes and assuming that the κ (κ') two (three)-site interaction scales as $\sim (1/2 + \delta)^\alpha$ with $\alpha = 2$ (3), respectively, one finds for the energy gain (per Mn ion) due to charge stacking along c direction for a 3D lattice:

$$\delta E = 6\kappa' \left(\frac{1}{2} + \delta \right)^3 \left[\sqrt{1 + \frac{\kappa^2}{36\kappa'^2(\frac{1}{2} + \delta)^2}} - 1 \right] - 2\delta^2 V. \quad (29)$$

The last term stands for the effective Coulomb repulsion at given charge modulation. With charge modulation sufficiently reduced $\delta \sim 0.2 - 0.3$ (see Fig. 14) the OO inter-plane coupling can stabilize charge-stacked phase ($\delta E > 0$). Such stabilization is strengthened (weakened) by increasing κ (κ') OO interaction, respectively. For smaller charge disproportion ($\delta \lesssim 0.1$) and considerable charge on $\text{Mn}^{3.5-\delta}$ sites the $\sim \kappa$ in-plane coupling [neglected in Eq. (28)] can also play an important role in the inter-plane charge modulation. However, when the CO is strongly reduced the orbital ground state is too complex to be analyzed analytically.

A further mechanism stabilizing the observed e_g charge stacking along the c direction results from the AF inter-plane superexchange interaction.²⁰ Yet, the magnetic interaction (J_{AF}) results mainly from the $t_{2g} - t_{2g}$ superexchange which is of the order of only a few meV.⁵² Thus, the antiferromagnetism in the c direction observed in most of the CE structures appears to be a *result* rather than the *origin* of the stacking pattern of the charge/orbital order.

IV. SUMMARY

We have investigated the potential of different electron-lattice mechanisms to stabilize the CE spin-orbital ordered phase in charge ordered half-doped manganites (filled with one e_g electron per two Mn ions). Our study is based on a generalized DE model containing the e_g orbital degrees of freedom, and also including inter-site Coulomb repulsion (V) and AF superexchange (J_{AF}) between core spins. The effect of three types of orbital interactions derived from the cooperative JT effect have been studied: (i) nearest neighbor JT-coupling, which is responsible for the alternating orbital order in undoped

LaMnO_3 , (ii) in addition second neighbor JT-interaction with a strength as expected for elastic strain, and (iii) a 2nd neighbor JT interaction which accounts for the breathing distortion of the Mn^{4+} octahedra and is in general stronger than (ii). A particular feature of this interaction, which has been proposed based on the classical model considerations in Sec. III D, are the displacements of the Mn^{4+} ions in the CE-phase.

We have studied these models employing finite temperature diagonalization on a $\sqrt{8} \times \sqrt{8}$ cluster with periodic boundary conditions, thereby keeping the translational invariance. The evolution of the different phases with temperature is monitored by the calculation of correlation functions for charge, orbital and spin, respectively. Starting out from the generalized FM Kondo lattice model (1) without any orbital interaction ($H_{\text{OO}} = 0$) we find the orbital correlations dominated by the $x^2 - y^2$ orbitals which are favored by the kinetic energy.^{43,44} This orbital state is characteristic for the metallic A-phase in wide-band manganites at half doping. For small AF superexchange interactions ($J_{\text{AF}} \ll t$) between t_{2g} core spins the FM state is found in the spin sector, while for larger values of J_{AF} the ground state is that of a regular 2 sublattice antiferromagnet. Even for large Coulomb repulsion V we found no evidence for C or CE structures for some intermediate values of the parameter J_{AF} . The inclusion of the nearest-neighbor JT-interaction (i), however, was found to stabilize the AF-C phase in a wide parameter range in the $V - J_{\text{AF}}$ phase diagram.

To obtain the more complex CE orbital and spin state not only the kinetic energy must be reduced by increasing the Coulomb repulsion V but also a further neighbor *antiferro-orbital* interaction must be included in the model. This interaction results from the electron-lattice coupling and is a generalization of the JT interaction which was found to play an important role in the parent LaMnO_3 compound.^{57,58} In CO compounds at quarter-filling the effect of the OO coupling will be dominated by interactions between further distant Mn neighbors. We have shown that such interactions can produce the CE structure in both *spin and orbital* sectors. In the case of the three-site effective interaction ($\sim \kappa'$) the zigzag chains are found to be stable not only for modest inter-site repulsion ($V \simeq 0.5t$) but even in the limit of $V = 0$ and provided κ is small, where the CO is induced entirely by the three-site orbital coupling (26). This effective next-nearest-neighbor OO coupling was derived taking into account the cooperative nature of both Mn^{3+} –O and Mn^{3+} – Mn^{4+} bonds length deformation. The free relaxation of the latter length leads in presence of CO to orbital alternation in planar directions, and the pattern of directed orbitals typical for the orbital CE structure appears. Consequently, with the help of the orbital topology,^{12,13} this gives rise to the CE AF spin ordering for realistic values for J_{AF} .

An important aspect of the second neighbor JT-interaction (iii) is its 3-site structure which involves a coupling to the charge at the Mn^{4+} ion. This implies

that the evolution of the CE orbital correlations with temperature are linked to the evolution of CO, while the magnetic CE correlations develop at lower temperature similar to $\text{Pr}_{1/2}\text{Ca}_{1/2}\text{MnO}_3$ ^{36,37}. This is different from (ii), where first CO develops, then OO and finally at lowest temperature AF spin order.

As discussed in Sec. III A we did not find the CE spin and/or orbital phase considering a pure electronic model, i.e., neglecting the electron-lattice coupling. Although, the topological effect combined with the DE mechanism leads to the preference of the CE over C phase when all e_g (bridge and corner) orbitals are degenerate,¹³ the situation is more complex when such degeneracy is lifted by JT lattice distortions. As described in the Appendix, one finds band insulators in both cases while the stability of the CE versus the C phase strongly depends on the crystal-field splittings ($E_z, \eta E_z \sim \lambda$).

An important issue is the degree of charge ordering in the CE phase. The CE spin-orbital structures obtained in our simulations appear in the regime of relatively strong CO, as inferred from our calculated charge correlation functions. Our calculations also suggest that the second neighbor JT coupling even for small or vanishing Coulomb repulsion can lead to a pronounced charge modulation. These results are consistent with the simple physical picture, that DE perpendicular to the FM chains must be strongly suppressed to allow AF superexchange to trigger the CE structure, which may not be the case for weak CO. On the other hand, a recent study by Mahadevan, Terakura and Sarma⁶⁶ based on the band structure approach arrived at the conclusion that the charge difference between the two Mn species in the CE phase is basically negligible, which would imply the absence of a significant breathing distortion of Mn^{4+} octahedra. Further experimental information on the degree of lattice distortion in the CE phase will certainly help to test the proposed JT based mechanism for the stability of the CE phase.

The charge modulations determined in our calculations may be influenced by numerical limitations which overestimate quantum fluctuations: (i) spins $S = 1/2$ are used to describe t_{2g} electrons; (ii) the calculations are made using a 2D cluster; (iii) the oxygen ions are not present explicitly in the cluster and thus only *dynamical* interactions are included (κ, κ'), which are mediated by oxygen displacements, while possible *static* lattice effects⁶⁷ are neglected. Certainly each of these approximations weakens the charge ordering and the spin-orbital order. It is, however, not straightforward to decide whether the region of the CE-phase in the phase diagram may grow or shrink, if quantum fluctuations are suppressed.

Finally we note that further neighbor JT interactions can also play an important role in the charge stripe formation at other commensurate carrier concentrations. For $x < 1/2$ ($x > 1/2$) the dominant coupling arises from the nearest- (next nearest-) neighbor OO interactions, respectively, with a pronounced electron-hole asymmetry present. In the latter case with small inter-site Coulomb

repulsion (V) the bi-stripe state⁶³ would be preferred while larger values of V would favor a “Wigner crystal” charge arrangement.⁶⁴

Acknowledgments

We would like to thank G. Khaliullin, M. Mayr and A. M. Oleś for stimulating discussions and valuable comments. J. B. acknowledges the support of the MPI für Festkörperforschung, Stuttgart. The financial support by the Polish State Committee of Scientific Research (KBN) of Poland, Project No. 5 P03B 055 20 is also acknowledged (J. B.).

APPENDIX: 1D BAND MODEL

A quite appealing explanation for the stability of the CE as compared to the C phase was suggested in Refs. 12,13 by considering a 1D model, where in the CE phase a gap opens as a consequence of a topological sign in the hopping matrix-elements. However, the intra-site Coulomb repulsion U (leading to some redistribution of the e_g charge) can destabilize the CE phase.^{68,69} Here we investigate how these arguments are modified when orbital degeneracy is lifted due to JT distortions. We consider the Hamiltonian:

$$H^{1D} = H_t + E_{z(b)} \sum_{i \in \text{corner}} T_i^z + \frac{1}{2} \eta E_{z(b)} \sum_{i \in \text{bridge}} n_i, \quad (\text{A.1})$$

which contains the kinetic energy H_t of an electron hopping along a FM chain¹³ with possible e_g level shift at the bridge sites ($\propto \eta E_{z(b)}$) and level splitting at corner sites ($\propto E_{z(b)}$) considered in two different orbital basis $\{|x\rangle, |z\rangle\}$ and $\{|a\rangle = \frac{1}{\sqrt{2}}(|x\rangle + |z\rangle), |b\rangle = \frac{1}{\sqrt{2}}(|x\rangle - |z\rangle)\}$. We assume that the energies of the bridge $3x^2 - r^2/3y^2 - r^2$ orbitals are located between the split energy levels at the corners assuming $|\eta| \leq 1$. Both kinds of level shifts can result from the lattice distortions. At the bridge site only the orbital $3x^2 - r^2$ ($3y^2 - r^2$) is considered while the orthogonal one $y^2 - z^2$ ($x^2 - z^2$), respectively, is decoupled in chain direction. In momentum space this leads to a 3×3 matrix problem:

$$H^{1D} = \sum_k \begin{pmatrix} d_{B,k}^\dagger \\ d_{x,k}^\dagger \\ d_{z,k}^\dagger \end{pmatrix}^T \begin{bmatrix} \eta E_z & W'_k & W_k \\ W'_k & E_z & 0 \\ W_k & 0 & -E_z \end{bmatrix} \begin{pmatrix} d_{B,k} \\ d_{x,k} \\ d_{z,k} \end{pmatrix}, \quad (\text{A.2})$$

where $W_k = -2t \cos k$ ($2t \cos k$) and $W'_k = -2\sqrt{3}t \sin k$ ($2\sqrt{3}t \cos k$) are the hopping elements for the CE (C) phase, respectively, in the $\{|x\rangle, |z\rangle\}$ orbital basis.

Calculating the band energies (see Fig. 15) one can easily determine the character of the stable phase. For the degenerate band model ($E_z = 0$) the C phase is metallic while in the CE phase a gap opens due to the *topological*

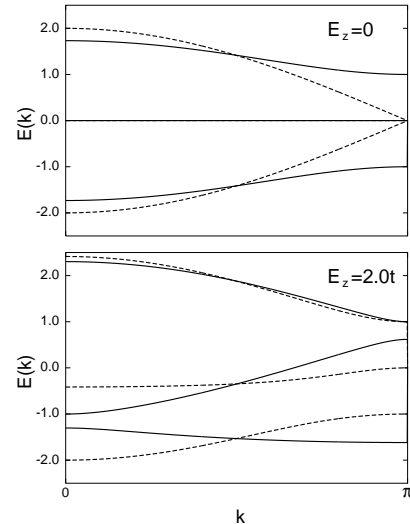


FIG. 15: Electron dispersion for the zigzag chain of the CE phase (solid lines) and for the linear chain of the C phase (dashed lines) calculated for different crystal-field splittings in the $\{|x\rangle, |z\rangle\}$ orbital basis at corner sites (E_z). The orbitals at the bridge sites are degenerate (assuming $\eta = 0$).

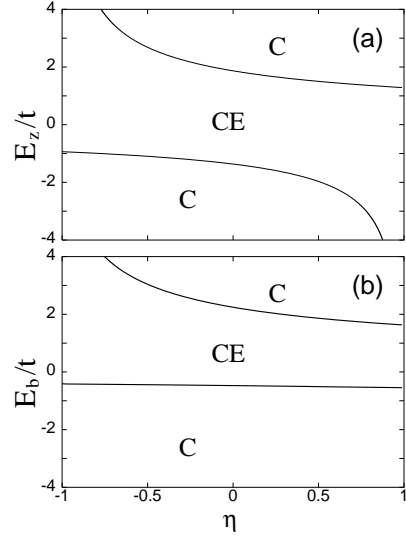


FIG. 16: Phase diagram of the chain model illustrating the stability of the CE against the C phase as function of the crystal-field splittings defined with respect to the orbital basis (a) $\{|x\rangle, |z\rangle\}$ and (b) $\{\frac{1}{\sqrt{2}}(|x\rangle \pm |z\rangle)\}$, respectively.

sign.^{12,13} The opening of the gap stabilizes the CE phase. When the degeneracy between $|x\rangle$ and $|z\rangle$ states at the corner sites ($E_z \neq 0$) is lifted, the C phase becomes insulating as well and for sufficiently large e_g level splittings it can have a *lower* energy than the CE phase when the chain is doped with one electron per two Mn sites [see Fig. 15(b)]. The region of stability of the CE phase increases for positive (negative) E_z when $\eta \rightarrow -1(1)$, respectively [see Fig. 16(a)]. Generally, the CE phase is sta-

bilized with respect to C, when the occupied bridge state approaches the lower energy level of the corner states. In a real half-doped crystal where in the CE phase Mn–O bond lengths shrink (expand) in the c direction [(a, b) plane], respectively, one would expect an energetic preference, due to the JT effect, for orbitals with stronger $x^2 - y^2$ than $3z^2 - r^2$ character. Thus, in the 1D model the relevant part of the phase diagram (Fig. 16) is the region with $E_z < 0$ and $\eta E_z < 0$, i.e., where the CE structure dominates.

To relate our mean-field considerations to the model from Sec. III B the stability of the CE phase versus C was also considered with level splitting at the corner sites defined with respect to the orbital basis $\{\frac{1}{\sqrt{2}}(|x\rangle \pm |z\rangle)\}$.

Such a splitting, directly related to the nearest-neighbor JT interaction (11) when $E_b > 0$, is operative in the C phase but vanishes by symmetry in the CE orbital phase. As shown in Fig. 16(b) the CE phase is stable for small splittings ($0 \lesssim E_b \lesssim 2t$) and in the $E_b > 0$, $\eta \rightarrow -1$ region. The latter is the relevant parameter range in the case of nearest neighbor JT interactions, and hence the model suggests the CE phase as stable phase. This, however, is in conflict with our numerical study of the 2D model, where only the C phase was found to be stable. As in 2D the nearest neighbor JT interaction stabilizes the C structure, whereas this interaction is frustrated in the CE phase. This effect is not included in the 1D model.

¹ For a review see: M. Imada, A. Fujimori, and Y. Tokura, Rev. Mod. Phys. **70**, 1039 (1998).

² Y. Tokura and N. Nagaosa, Science **288**, 462 (2000).

³ Y. Moritomo, H. Kuwahara, Y. Tomioka, Y. Tokura, Phys. Rev. B **55**, 7549 (1997).

⁴ R. Kajimoto, H. Yoshizawa, Y. Tomioka, and Y. Tokura, Phys. Rev. B **66**, 180402 (2002).

⁵ B. J. Sternlieb, J. P. Hill, U. C. Wildgruber, G. M. Luke, B. Nachumi, Y. Moritomo, and Y. Tokura, Phys. Rev. Lett. **76**, 2169 (1996).

⁶ Y. Murakami, H. Kawada, H. Kawata, M. Tanaka, T. Arima, Y. Moritomo, and Y. Tokura, Phys. Rev. Lett. **80**, 1932 (1998).

⁷ K. Nakamura, T. Arima, A. Nakazawa, Y. Wakabayashi, and Y. Murakami, Phys. Rev. B **60**, 2425 (1999).

⁸ E. O. Wollan and W. C. Koehler, Phys. Rev. **100**, 545 (1955).

⁹ J. B. Goodenough, Phys. Rev. **100**, 564 (1955).

¹⁰ R. Kilian and G. Khaliullin, Phys. Rev. B **60**, 13 458 (1999).

¹¹ K. I. Kugel and D. I. Khomskii, Zh. Eksp. Teor. Fiz. **64**, 1429 (1973) [Sov. Phys. JETP **37**, 725 (1973)]; Usp. Fiz. Nauk **136**, 621 (1982) [Sov. Phys. Usp. **25**, 232 (1982)].

¹² I. V. Solovyev and K. Terakura, Phys. Rev. Lett. **83**, 2825 (1999).

¹³ J. van den Brink, G. Khaliullin, and D. Khomskii, Phys. Rev. Lett. **83**, 5118 (1999).

¹⁴ I. V. Solovyev, Phys. Rev. B **63**, 174406 (2001).

¹⁵ T. Mutou and H. Kontani, Phys. Rev. Lett. **83**, 3685 (1999).

¹⁶ G. Jackeli, N. B. Perkins, and N. M. Plakida, Phys. Rev. B **62**, 372 (2000).

¹⁷ Z. Shu, J. Dong, and D. Y. Xing, Phys. Rev. B **63**, 224409 (2001).

¹⁸ Z. Popović and S. Satpathy, Phys. Rev. Lett. **88**, 197201 (2002).

¹⁹ T. Mizokawa and A. Fujimori, Phys. Rev. B **56** R493 (1997).

²⁰ S. Yunoki, T. Hotta, and E. Dagotto, Phys. Rev. Lett. **84**, 3714 (2000).

²¹ T. Hotta, Y. Takada, H. Koizumi, and E. Dagotto, Phys. Rev. Lett. **84**, 2477 (2000).

²² T. Hotta, A. Feiguin, and E. Dagotto, Phys. Rev. Lett. **86**, 4922 (2001).

²³ R. Y. Gu and C. S. Ting, Phys. Rev. B **65**, 214426 (2002).

²⁴ A. Weiße and H. Fehske, Eur. Phys. J. B **30**, 487 (2002).

²⁵ S. B. Wilkins *et al.*, Phys. Rev. Lett. **91**, 167205 (2003).

²⁶ Y. Tomioka, A. Asamitsu, Y. Moritomo, H. Kuwahara, and Y. Tokura, Phys. Rev. Lett. **74**, 5108 (1995).

²⁷ H. Kawano, R. Kajimoto, H. Yoshizawa, Y. Tomioka, H. Kuwahara, and Y. Tokura, Phys. Rev. Lett. **78**, 4253 (1997).

²⁸ M. v. Zimmermann, C. S. Nelson, J. P. Hill, Doon Gibbs, M. Blume, D. Casa, B. Keimer, Y. Murakami, C.-C. Kao, C. Venkataraman, T. Gog, Y. Tomioka, and Y. Tokura, Phys. Rev. B **64**, 195133 (2001).

²⁹ M. Kubota, H. Yoshizawa, Y. Moritomo, H. Fujioka, K. Hirota, and Y. Endoh, J. Phys. Soc. Jpn **68**, 2202 (1999).

³⁰ D. N. Argyriou *et al.*, Phys. Rev. B **61**, 15269 (2000).

³¹ S. Ishihara and S. Maekawa, Phys. Rev. B **62**, 5690 (2000).

³² C. H. Chen, S. Mori, and S.-W. Cheong, Phys. Rev. Lett. **83**, 4792 (1999).

³³ S. Larochelle, A. Mehta, N. Kaneko, P. K. Mang, A. F. Panchula, L. Zhou, J. Arthur, and M. Greven, Phys. Rev. Lett. **87**, 095502 (2001).

³⁴ C. Zener, Phys. Rev. **82**, 403 (1951); P. W. Anderson and H. Hasegawa, *ibid.* **100**, 675 (1955). P. -G. de Gennes, Phys. Rev. **118**, 141 (1960).

³⁵ T. Hotta, A. L. Malvezzi, and E. Dagotto, Phys. Rev. B **62**, 9432 (2000).

³⁶ H. Kajimoto, H. Yoshizawa, Y. Tomioka, and Y. Tokura, Phys. Rev. B **63**, 212407 (2001).

³⁷ M. v. Zimmermann *et al.*, Phys. Rev. Lett. **83**, 4872 (1999).

³⁸ J. Geck, D. Bruns, C. Hess, R. Klingeler, P. Reutler, M. v. Zimmermann, S.-W. Cheong, and B. Büchner, Phys. Rev. B **66**, 184407 (2002).

³⁹ A. Moreo, S. Yunoki, and E. Dagotto, Science **283**, 2034 (1999).

⁴⁰ P. G. Radaelli, D. E. Cox, M. Marezio, and S.-W. Cheong, Phys. Rev. B **55**, 3015 (1997).

⁴¹ D. I. Khomskii and K. I. Kugel, Phys. Rev. B **67**, 134401 (2003).

⁴² M. J. Calderon, A. J. Millis, and K. H. Ahn, Phys. Rev. B **68**, R100401 (2003).

⁴³ P. Horsch, J. Jaklić, and F. Mack, Phys. Rev. B **59**, 6217 (1999).

⁴⁴ F. Mack and P. Horsch, Phys. Rev. Lett. **82**, 3160 (1999).

⁴⁵ M. Uehara, S. Mori, C. H. Chen, and S.-W. Cheong, Na-

ture **399**, 560 (1999).

⁴⁶ Y. Okimoto *et al.*, Phys. Rev. B **59**, 7401 (1999).

⁴⁷ J. H. Jung *et al.*, Phys. Rev. B **62**, 481 (2000).

⁴⁸ F. Mack, Ph. D. thesis, University of Stuttgart, 1999.

⁴⁹ J. Jaklič and P. Prelovšek, Adv. Phys. **49**, 1 (2000).

⁵⁰ A. E. Bocquet, T. Mizokawa, T. Saitoh, H. Namatame, and A. Fujimori, Phys. Rev. B **46**, 3771 (1992); T. Saitoh, A. E. Bocquet, T. Mizokawa, H. Namatame, A. Fujimori, M. Abbate, Y. Takeda, and M. Takano, *ibid.* **51**, 13 942 (1995); S. Satpathy, Zoran S. Popovic and Filip R. Vukajlovic, Phys. Rev. Lett. **76**, 960 (1996).

⁵¹ S. Ishihara, J. Inoue, and S. Maekawa, Phys. Rev. B **55**, 8280 (1997).

⁵² L. F. Feiner and A. M. Oleš, Phys. Rev. B **59**, 3295 (1999).

⁵³ A. J. Millis, Nature **392**, 147 (1998).

⁵⁴ J. Bała, A. M. Oleś, and G. A. Sawatzky, Phys. Rev. B **65**, 184414 (2002).

⁵⁵ J. van den Brink, P. Horsch, F. Mack, and A. M. Oleś, Phys. Rev. B **59**, 6795 (1999).

⁵⁶ U. Yu, Y. V. Skrypnyk, and B. I. Min, Phys. Rev. B **61**, 8936 (2000).

⁵⁷ A. J. Millis, Phys. Rev. B **53**, 8434 (1996).

⁵⁸ K. H. Ahn and A. J. Millis, Phys. Rev. B **58**, 3697 (1998).

⁵⁹ To account for local non-central OO interactions one should use full sets of coordinates for each ion in Mn⁴⁺ octahedra and include nonlinear lattice effects.

⁶⁰ J. van den Brink and D. I. Khomskii, Phys. Rev. B **63**, 140416 (2001); R. Maezono and N. Nagaosa, *ibid.* **62**, 11 576 (2000).

⁶¹ J. Bała, A. M. Oleś, and P. Horsch, Phys. Rev. B **65**, 134420 (2002).

⁶² We note that $K_1 = \tilde{K}_1 b^2$ and $\lambda = \tilde{\lambda} b$; hence in conventional notation these values correspond to $\tilde{K}_1 \approx 13 \text{ eV}/\text{\AA}^2$ and $\tilde{\lambda} \approx 1.5 \text{ eV}/\text{\AA}$.

⁶³ S. Mori, C. H. Chen, and S.-W. Cheong, Nature **392**, 473 (1998).

⁶⁴ P. G. Radaelli, D. E. Cox, L. Capogna, S.-W. Cheong, M. Marezio, Phys. Rev. B **59**, 14440 (1999).

⁶⁵ Deviations from this rule are observed when Re and A cations order; see T. Arima *et al.*, Phys. Rev. B **66**, 140408 (2002).

⁶⁶ P. Mahadevan, K. Terakura, and D. D. Sarma, Phys. Rev. Lett. **87**, 066404 (2001).

⁶⁷ J. Bała and A. M. Oleś, Phys. Rev. B **62**, 6085 (2000).

⁶⁸ S.-Q. Shen, Phys. Rev. Lett. **86**, 5842 (2001).

⁶⁹ M. Cuoco, C. Noce, and A. M. Oleś, Phys. Rev. B **66**, 094427 (2002).